Article

Vertical Integration of Nitride Laser Diodes and Light Emitting Diodes by Tunnel Junctions

Marcin Siekacz *, Grzegorz Muziol, Henryk Turski, Mateusz Hajdel, Mikolaj Żak, Mikolaj Chlipała, Marta Sawicka, Krzesimir Nowakowski-Szkudlarek, Anna Feduniewicz-Żmuda, Julita Smalc-Koziorowska, Szymon Stańczyk and Czeslaw Skierbiszewski

Institute of High Pressure Physics, Polish Academy of Sciences, Sokolowska 29/37, 01-142 Warsaw, Poland; gmuziol@unipress.waw.pl (G.M.); henryk@unipress.waw.pl (H.T.); hajdel@unipress.waw.pl (M.H.); mzak@unipress.waw.pl (M.Ż.); mik@unipress.waw.pl (M.C.); sawicka@unipress.waw.pl (M.S.); krzesimir.szkudlarek@unipress.waw.pl (K.N.-S.); ania_f@unipress.waw.pl (A.F.-Ż.); julita@unipress.waw.pl (J.S.-K.); szymons@unipress.waw.pl (S.S.); czeslaw@unipress.waw.pl (C.S.)
* Correspondence: msiekacz@unipress.waw.pl; Tel.: +48-22-876-0324

Abstract: We demonstrate the applications of tunnel junctions (TJs) for new concepts of monolithic nitride-based multicolor light emitting diode (LED) and laser diode (LD) stacks. The presented structures were grown by plasma-assisted molecular beam epitaxy (PAMBE) on GaN bulk crystals. We demonstrate a stack of four LDs operated at pulse mode with emission wavelength of 453 nm. The output power of 1.1 W and high slope efficiency of 2.3 W/A is achieved for devices without dielectric mirrors. Atomically flat surface after the epitaxy of four LD stack and low dislocation density is measured as a result of proper TJ design with optimized doping level. The strain compensation design with InGaN waveguides and AlGaN claddings is shown to be crucial to avoid cracking and lattice relaxation of the 5 μm thick structure. Vertical connection of n-LDs allows for cascade emission of photons and increases the quantum efficiency n-times. The two-color (blue and green) LEDs are demonstrated. Application of TJs simplifies device processing, reducing the need for applications of *p*-type contact. The key factor enabling demonstration of such devices is hydrogen-free PAMBE technology, in which activation of buried *p*-type layers is not necessary.

Keywords: molecular beam epitaxy; nitrides; laser diode; tunnel junction

1. Introduction

The main breakthrough in III-N optoelectronic devices was related with the development of the *p*-type Mg doped layers [1]. The relatively poor *p*-type conductivity and fabrication of low resistance ohmic *p*-type contacts are still among the most challenging issues in nitrides. Recently, increased attention has been dedicated to the interband tunnel junctions (TJs) [2] for the efficient conductivity conversion from *p*-type to *n*-type in III-nitride devices [3–7]. Application of tunnel junctions (TJs) offers more freedom in device design—e.g., it eliminates the need for *p*-type contact deposition [5,8–10]. However, the utilization of TJs in wide band semiconductors is a counterintuitive approach because it is well known that the tunneling probability through *p–n* junction decreases exponentially with the energy gap. The additional complication, which slowed down the progress of the nitride TJs' development, was related with the *p*-type doping procedure used by metal-organic vapor phase epitaxy (MOVPE), the dominant technology for the nitride optoelectronics devices. In MOVPE it is difficult to activate the *p*-type conductivity in the (In)GaN:Mg layers that are buried below *n*-type layers due to the fact that diffusion of hydrogen is completely blocked through *n*-type layers [6,11–13].

The issue with the activation of the Mg doped *p*-type layers is not present for the hydrogen-free plasma-assisted molecular beam epitaxy (PAMBE) technology. In PAMBE, hydrogen is not incorporated into GaN:Mg layers, therefore there is no passivation of Mg dopant and no need for post-growth annealing. For this reason, PAMBE seems to be much better suited than MOVPE for practical realization of the vertical devices with buried *p*-type layers [14]. Recently, making use of PAMBE, it was shown that TJs' resistance for wide bandgap semiconductors can be significantly reduced by making use of the piezoelectric fields in the region of the junction [3,7]. The use of piezoelectric fields and heavy *p*- and *n*-type doping levels allowed us to reduce the TJs' resistance to a level appropriate for a demonstration of the continuous wave operation of nitride laser diodes (LDs) [14].

Efficient TJs enable the realization of different vertical designs of optoelectronic devices. Namely: (1) stacks of LDs or (2) multicolor light emitting diodes (LEDs). The multicolor LEDs can pave a way for efficient low energy consumption matrix displays. The stack of LDs is very attractive for many applications where pulse mode operation is required, such as gas sensing, printing and environment pollution control, or light detection and ranging (LIDAR) in cartography, automotive and industrial systems [15]. It can be very cheap and viable alternative to the arrays of LD bars. It provides much simpler coupling of the light coming from the stack of LDs with external optics than from arrays of LDs, since the spatial separation between vertical devices is two orders of magnitude smaller than for arrays of LD bars. The simultaneous operation of a cascade of *n* LDs increases the slope efficiency (SE) of the full device *n*-times, which makes high-power lasing conditions accessible for smaller currents. In addition, the level of catastrophic optical damage (COD) is *n*-times higher in comparison with a single LD. In spite of the increasing interest, there is only one report on a stack of two III-N LDs grown by MOCVD, which shows very weak evidence of simultaneous laser action from both active regions [16]. This is probably due to difficulties with Mg acceptors activation in buried *p*-type layers. Making use of the PAMBE technology we already demonstrated that it is possible to grow monolithically a stack of two LDs operating at two different wavelengths [17].

In this work we will go a step further and investigate a stack of four LDs operating at the same frequency interconnected by TJs. We demonstrate that by making use of the strain compensation concept, it is possible to grow a 5 μm nitride structure containing thick InGaN and AlGaN layers without generation of lattice relaxation. In addition, we demonstrate the potential of PAMBE for growth of vertically integrated multicolor LEDs.

2. Materials and Methods

2.1. Laser Diodes

The epitaxial structure of the LD stack presented in this work was grown entirely by PAMBE on bulk (0001) GaN crystal with the miscut of 0.5°. The substrate was a commercially available Ammono-GaN crystal with low threading dislocation density (TDD) about 10^5 cm^{-2} [18]. The structure consists of four LD segments interconnected by TJs, as shown schematically in Figure 1a,b. At the top of each LD structure the TJ is placed, which makes it ready for the growth of a subsequent LD. The TJs are located far away (approximately 500 nm) from the waveguides of the LDs to avoid generation of additional optical losses due to heavy *p*-type doping. For such a design, the calculated optical mode overlap with the TJ is extremely low in the order of 10^{-7}. Assuming even a high absorption loss of $\alpha = 4000$ cm^{-1}, the resulting optical loss should be at the level of 0.01 cm^{-1}, which is negligible.

Details of the epitaxial structure of one LD segment with a TJ on top are presented in Figure 1b. At the bottom of each LD there is a 400 nm $Al_{0.05}Ga_{0.95}$N:Si cladding (except the most bottom laser diode, LD4, in which the cladding thickness was 700 nm). The LD segment consists of a 220 nm $In_{0.04}Ga_{0.96}$N waveguide and a 25 nm $In_{0.17}Ga_{0.83}$N single quantum well (SQW) [19]. Above the waveguide a 20 nm $Al_{0.14}Ga_{0.86}$N:Mg electron blocking layer (EBL) is placed. EBL is doped with Mg at the level of 2×10^{19} cm^{-3}, followed by upper $Al_{0.05}Ga_{0.95}$N:Mg cladding (Mg doping level is 1×10^{18} cm^{-3}). The TJ region consists of 60 nm $In_{0.02}Ga_{0.98}$N:Mg, a 10 nm $In_{0.17}Ga_{0.83}$N quantum well

(QW), and 20 nm $In_{0.02}Ga_{0.98}$N:Si. The $In_{0.02}Ga_{0.98}$N barriers are doped with Mg and Si at the levels of 2×10^{19} cm^{-3} and 4×10^{19} cm^{-3}, respectively. First, 5 nm of the QW is heavily doped with Mg at the level of 1.6×10^{20} cm^{-3} while the following 5 nm of the QW is *n*-type doped at the level of 1.8×10^{20} cm^{-3}. The Mg and Si doping profiles in TJs were optimized to achieve atomically flat surface without defects, which is essential for the growth of the subsequent devices on top within the stack.
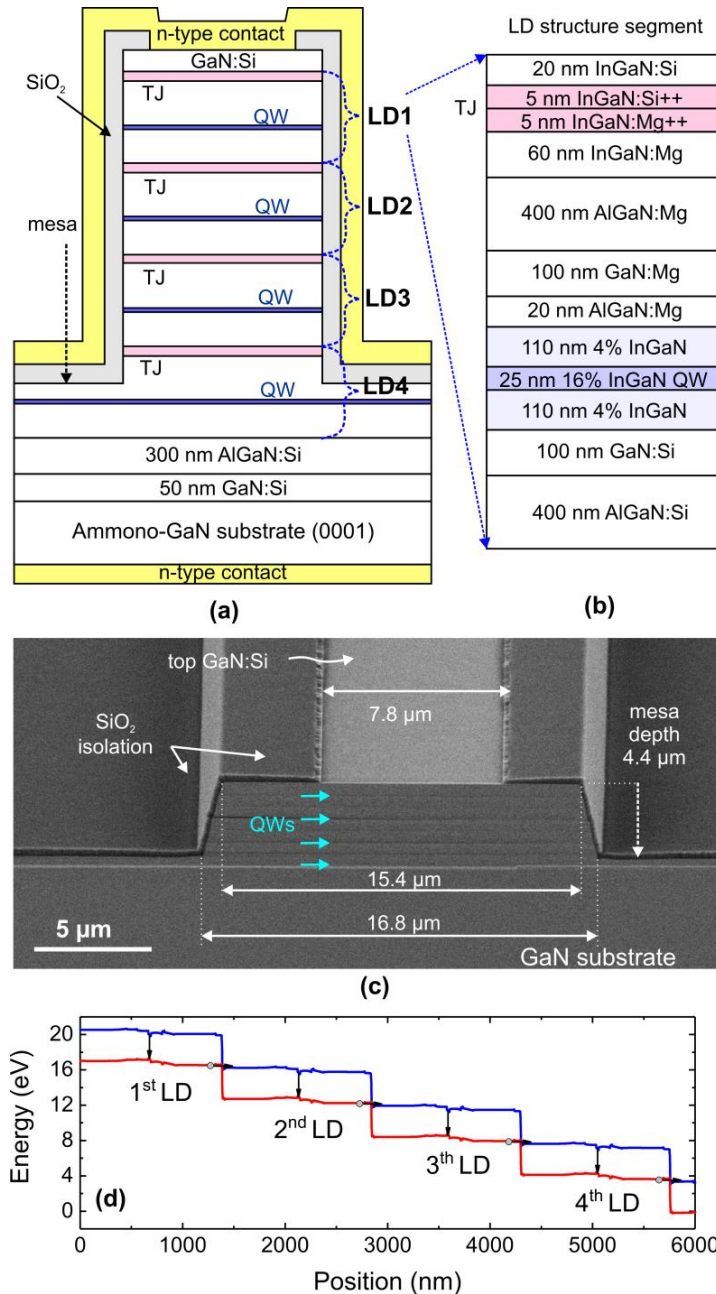

Figure 1. (**a**) Schematic image of the processing design of a stack of four laser diodes (LDs) grown by plasma-assisted molecular beam epitaxy (PAMBE); (**b**) detailed layer structure of a single LD segment; (**c**) scanning electron microscopy (SEM) image of laser mesa viewed at 45° at cleaved laser facet; (**d**) band diagram of stack of four LDs.

The growth conditions of the four LD stack were the same as for a single LD and they are described in detail elsewhere [20]. The growth temperatures were 730 °C for GaN and 650 °C for InGaN layers, respectively. The temperature on the grown surface was monitored (and adjusted if necessary) by laser reflectometry described in detail in [21]. We would like to mention here that the entire structure

was grown on planar GaN substrate without special patterning applied to reduce strain caused by thick AlGaN claddings [22]. The growth of thick AlGaN claddings usually leads to the cracking of the structures. Application of InGaN waveguides surrounded by AlGaN claddings results in strain compensation and allows us to grow such thick structures without lattice relaxation. It is important to stress here, that such an approach allows us also to achieve flat wafers, which is important for device yield during the processing of lasers.

The LDs were processed as a ridge waveguide with the dimensions of $15\,\mu m \times 1000\,\mu m$. The $4.4\,\mu m$ deep mesa was formed by reactive-ion etching (RIE) through active regions of the 3 LDs and reaching almost the EBL of the fourth LD (see Figure 1c). The mesa was covered by SiO_2 dielectric. To ensure that the metal contacts will not make a short cut on the mesa sidewalls, the top of the mesa region was also covered partially by SiO_2 (see Figure 1c). The overlap of the dielectric on the mesa surface reduces the size of the metal contact. The metal contact width is about $8\,\mu m$, while mesa size is $15\,\mu m$. It could be a challenge for standard LDs with *p*-type contact, in which low conductivity of *p*-type material restricts lateral carrier distribution to distances below $1\,\mu m$. This could lead to non-uniform current spreading through such processed LDs. However, in our design, the electrons can easily travel from metallization to the mesa edges (*n*-type contact: Ti/Al/Ni/Au) because the current spreading layer is *n*-type. The processed devices were cleaved and tested without dielectric mirror coatings.

The band diagram for the studied LD stack is shown in Figure 1d. Arrows indicate the electron recombination in the QWs and tunneling though the TJs.

2.2. Light Emitting Diodes

The schematic diagram of the stack of 2 LEDs operated at different wavelengths for color mixing is presented in Figure 2. The schematic working idea shown in Figure 2a explains that the power supply of the studied device can be applied either to the whole structure or separately to each of the LEDs. The structure was grown on conductive commercial GaN substrate (Saint Gobain Lumilog) with TDDs in the range from 5×10^6 to 1×10^7 cm^{-2}. Layer sequence is presented in Figure 2b. After 30 nm $In_{0.08}Ga_{0.92}N$ layer, two 2.8 nm $In_{0.23}Ga_{0.77}N$ QWs were grown with 20 nm $In_{0.08}Ga_{0.92}N$ barriers, followed by 20 nm $Al_{0.15}Ga_{0.85}N$:Mg EBL, 100 nm GaN:Mg and the first TJ. Above the first TJ (TJ1), the 100 nm $In_{0.02}Ga_{0.98}N$ doped with Si at the level 5×10^{18} cm^{-3} was located. Then, the second LED was grown—with In content of 17% inside two 2.8 nm InGaN QWs. On top of the second LED, the second TJ (TJ2) was located, followed by 100 nm GaN doped Si at the level of 5×10^{18} cm^{-3}. The upper GaN:Si and 100 nm $In_{0.02}Ga_{0.98}N$:Si located between the bottom (green) and top (blue) LEDs were used for efficient lateral current spreading. The TJ design (thickness of the layers) are the same as for the stack of LDs described before. The differences are in the n- and *p*-type doping of the 10 nm TJ QW region (for TJ details, see Figure 1b). For TJ1, we used moderate doping levels (like for LDs described above) to provide high crystal quality, while for TJ2 the doping was increased: $N_{Si} = 4 \times 10^{21}$ cm^{-3}, $N_{Mg} = 5 \times 10^{20}$ cm^{-3}.

Figure 2c presents a high-angle annular dark-field scanning transmission electron microscopy (HAADF STEM) image of the studied two-color LED structure. High indium content layers, such as InGaN QWs and TJs, are brighter than GaN and AlGaN layers. Sharp interfaces and no extended defects indicate high quality growth. The devices ($350 \times 350\,\mu m^2$ mesa size) were separated by deep dry etching by reactive ion etching (RIE), down to the substrate. The schematic picture of the LED after processing will be presented in the following part of the paper.

The band diagram for the studied structure is shown in Figure 2d. Again, similarly to the LD stack band diagram shown in Figure 1d, the arrows indicate the electron recombination in QWs and tunneling though the TJs.
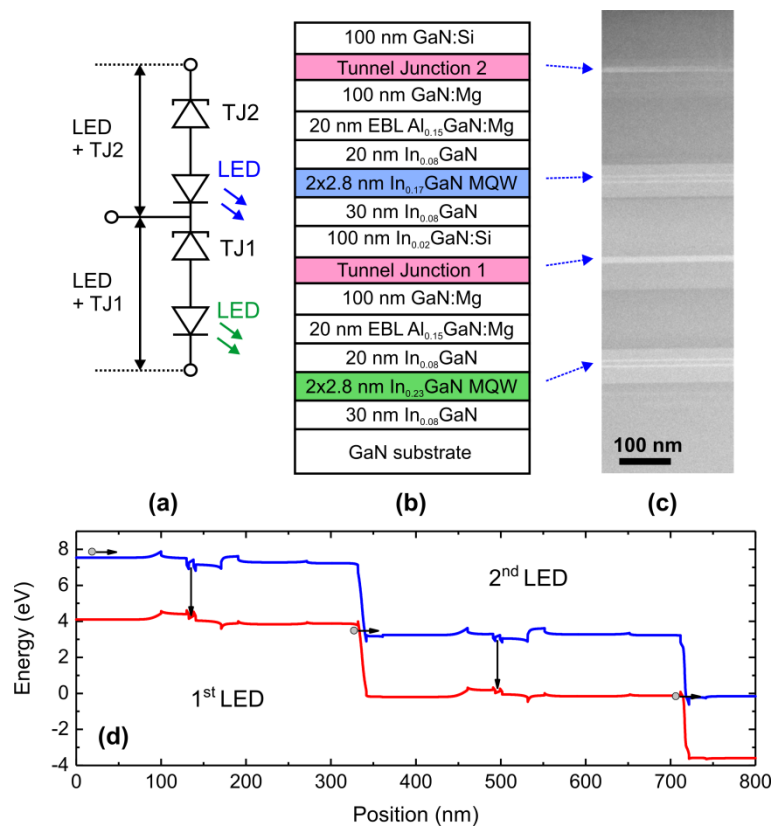
Figure 2. (**a**) Schematic diagram and (**b**) layer sequence of two-color light emitting diode (LED) structure. (**c**) High-angle annular dark-field scanning transmission electron microscopy (HAADF STEM) image presenting the studied two-color LED structure. (**d**) Band structure of two-color LED.

3. Results and Discussion

3.1. Laser Diodes

The LDs were operated with 200 ns long pulses and a repetition rate of 1 kHz. The light–current (L–I) characteristics of the cascade of four LDs are shown in Figure 3a. Three lasing thresholds had been observed: the first one at a current density of 3.8 kA/cm^2 with a slope efficiency of 0.8 W/A; the second one occurred at 5.9 kA/cm^2 and the observed slope efficiency was equal to 1.5 W/A; the third one was at 6.4 kA/cm^2 and the slope efficiency increased to 2.3 W/A. The multiplications of the slope efficiency indicate that the same electrons (and holes) are used three times to generate light—once in each of the three LDs.

To verify the observation of lasing from the LDs' stack, we measured near-field patterns collected using a Gaussian beam telescope setup [23]. Strong filamentation is observed as expected for wide-ridge LDs [24]. At j = 3.8 kA/cm^2, there is only a single near-field pattern for LD1 visible (see Figure 3b). Above the second threshold a second near-field pattern appears below. For current densities higher than 6.4 kA/cm^2, a third peak in the near-field pattern is observed. Further increase of the current density does not change this pattern. This experiment shows that the LDs start the lasing action in the following order: LD1, LD2 and LD3. Furthermore, we observed that LD4 was not lasing. We suspect that the reason why LD4 was not lasing is that the mesa was too shallow. The distance from the surface to the EBL of LD4 is 4.8 µm, while the etching depth measured by SEM (see Figure 1c) was 4.4 µm. Therefore, one can expect very different waveguiding properties for LD4 in comparison to LD1–LD3, which were etched through the whole structure. For LD1–LD3, the optical mode is confined laterally by SiO$_2$ deposited on the sides of the mesa, while for LD4 the optical mode can spread laterally to unpumped regions (see Figure 1c). This geometry increases the optical confinement factor for LD1–LD3

and increases the internal optical losses for LD4. Therefore, we expect a substantial increase in the lasing threshold current density for LD4.

The maximum optical power obtained for the studied structure was 1.1 W per laser facet and can be further increased using dielectric coatings. Application of this design for *n*-LDs interconnected by (*n*−1) TJs will allow us to increase SE *n*-times. This construction paves a way to achieving III-nitride high-power pulse laser diode stacks for LIDAR applications.
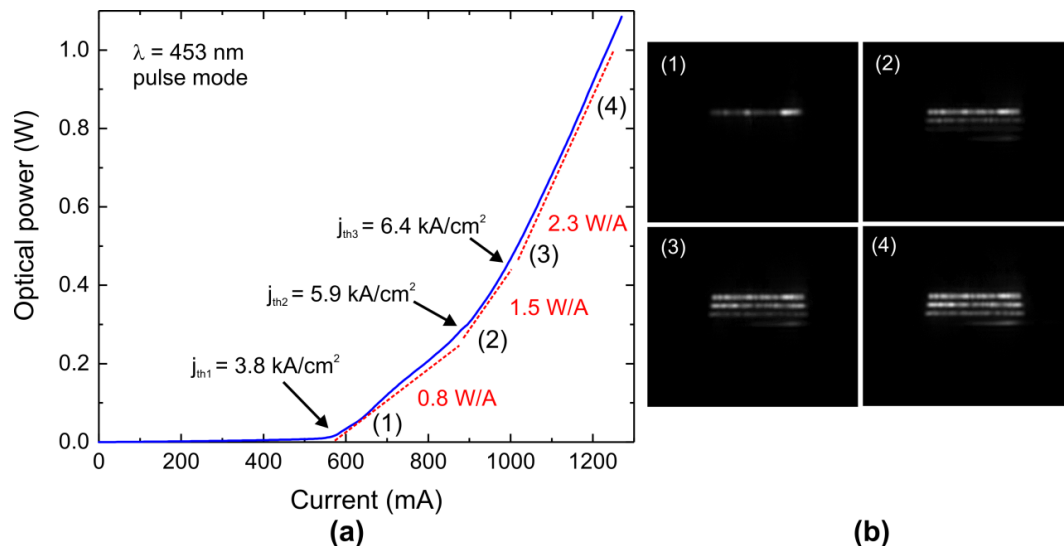

Figure 3. (**a**) The light–current characteristics of the stack of four LDs structure grown by PAMBE. Three lasing thresholds are observed. Total slope efficiency follows the number of lasing devices multiplied by slope efficiency of the first LD; (**b**) the near-field patterns collected by Gaussian beam telescope setup for the lasing regions (1)–(4) denoted in the light–current characteristics.

The important part in the design of the LDs' stack presented in this work is related with optimization of the TJ design and epitaxy. The TJ should have low resistance and the growth should not introduce additional structural defects. In this work, we applied TJ design which consists of InGaN QW to increase the current tunneling probability [3,7]. The *p*- and *n*-type doping levels were optimized to provide low serial resistance of a TJ. However, the *p*-type and *n*-type doping are limited by inherent physical properties or by structural deterioration. For the *p*-type Mg doping, above the doping level 2—5×10^{19} cm^{-3}—the self-compensation process is observed, which reduces efficiency of magnesium as an acceptor [25,26]. Contrary to *p*-type, the *n*-type doping is still efficient for very high Si doping levels. Indeed, the increase in the Si doping reduces the tunnel junction resistance, however, for concentrations at the order of 5×10^{20} cm^{-3} a deterioration of the surface morphology is observed. The mechanism of this process is probably related to the Si masking effect when the surface is exposed to the very high Si flux. The surface morphology of our four LDs' stack is shown in Figure 4a. The *n*-type Si doping in TJ equals to 1.8×10^{20} cm^{-3}. For higher *n*-type doping—above 5×10^{20} cm^{-3}—surface roughening is observed, and many dislocations are generated, as shown in Figure 4b. The TJ presented in Figure 4b, was used for our first demonstration of TJ LDs [14]. Heavy Si doping allowed us to achieve a very low resistance TJ; however, high defect density and rough surface morphology would not allow for the growth of subsequent LDs. Note that the surface root mean square roughness measured by atomic force microscope (AFM) at 5×5 µm^2 scans is 0.29 nm for the four LDs' stack with optimized TJs and 2.34 nm for the single LD with the highly doped TJ on top of it, see Figure 4a,b, respectively.

The defect density of the four LDs' stack was studied. We used defect-selective etching (DSE) in molten KOH–NaOH eutectics at 450 °C for 15 min. After DSE, etch pit density (EPD) was evaluated using optical microscope images. For a given image, the etch pits are counted per known area and

thus their density is easily calculated. An example of the optical microscope image of the four LDs' stack surface after DSE is shown in Figure 4c, in which the pits (some are marked by arrows) can be observed. In Figure 4c, 24 pits on the area of 13.4 μm^2 result in EPD of 1.8×10^6 cm^{-2}. Note that some pits have a flat bottom that may indicate dislocations generated during epitaxy of the four LDs' stack. The etch pits corresponding to the dislocations which originate from the substrate are denoted with black arrows and their density matches approximately the TDD of the GaN substrates used. The overall low defect density revealed by the DSE shows that the stacking of LDs by TJ using PAMBE is a promising technology for high-power pulse laser diodes [27].
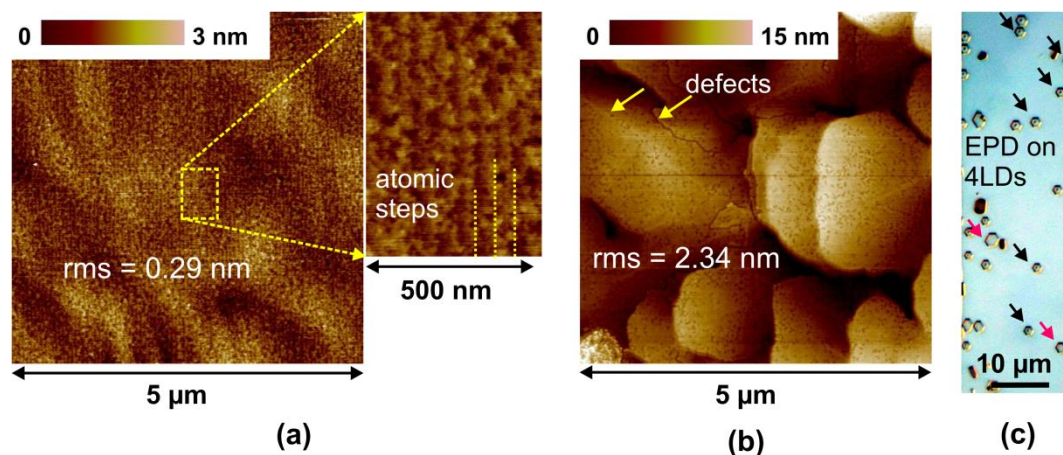

Figure 4. Surface morphology of (**a**) stack of 4 LDs with Si doping in TJ of 1.8×10^{20} cm^{-3}; (**b**) single LD with heavy Si doping in TJ above 5×10^{20} cm^{-3}. (**c**) Optical microscope image of the studied 4 LDs' epitaxial structure after defect-selective etching. Etch pit density is 1.8×10^6 cm^{-2}. Some of etch pits are flat-bottomed, indicated by pink arrows.

3.2. Multicolor Light Emitting Diodes

We analyzed the properties of the device that consisted of two standard LED structures emitting at true blue and green range, interconnected and capped with heavily doped $In_{0.02}Ga_{0.98}N/In_{0.17}G_{0.83}aN/In_{0.02}Ga_{0.98}N$ TJs. The device structure is presented in Figure 2. The electroluminescence taken at different currents is presented in Figure 5 and two emission lines centered at 466 nm and 530 nm are visible. For the bottom and top of the LEDs' stack we used *n*-type Ti/Al/Ni/Au contacts. Two-color LED operates at reasonably low voltages of about 8 V for currents around 150 mA. It is important to point out that the light is extracted through the upper LED region which is not covered by metallization. This is characteristic for TJ LEDs—since electrons are more mobile than holes and TJ enables efficient horizontal current spreading. As an example, in Figure 6 we demonstrate the electroluminescence of our TJ LED devices with different shapes of upper contact metallization which defines the output light pattern.

Further development of such device, when adding the third LED, emitting red color, could lead to a phosphorous-free white LED. We would like to stress here that vertical interconnection by TJs also simplifies the processing of individually addressed LED devices. This could be interesting for the future design of multicolor LED matrix displays. In Figure 7a, a schematic diagram of the etched structure is presented. To obtain middle contact we partially etched the structure down about 400 nm and deposited *n*-type contact (Ti/Al/Ni/Au) to $In_{0.02}Ga_{0.98}N$:Si doped layer (for structure details see Figure 2). It is a great advantage, since there is no need to fabricate *p*-type contacts on the etched surface of the device, which is a challenging issue. Using this configuration, we can bias each LED individually. In Figure 7b, the Current–Voltage (I–V) characteristics of the upper (blue), bottom (green) and both LEDs are presented. We observe a higher turn-on voltage for the green diode (i.e., TJ1 + green LED) than for the blue diode (TJ2 + blue LED). This effect is probable due to the higher voltage drop on TJ1 in comparison to TJ2. In addition, for the green diode, the increase in turn-on voltage can be caused

by stronger piezoelectric field related to higher indium content in green QWs. As was mentioned before, application of TJs simplifies preparation of the contacts on the etched surface. Here, we applied *n*-type contact between green and blue LEDs. The slope of the I–V curve above the turn-on voltage is a measure of the serial resistance of the device. The green LED and both green and blue LEDs have a similar slope. The increased serial resistance for blue LED is due to lateral resistance of the *n*-type layer located below the blue LED. The electrons must travel from the bottom contact of the blue LED for several microns through $In_{0.02}Ga_{0.98}N$:Si layer doped at moderate values (see Figures 2b and 7a). We can eliminate this effect by increased *n*-type doping of this layer and/or by smaller spacing between mesa and the bottom contact.
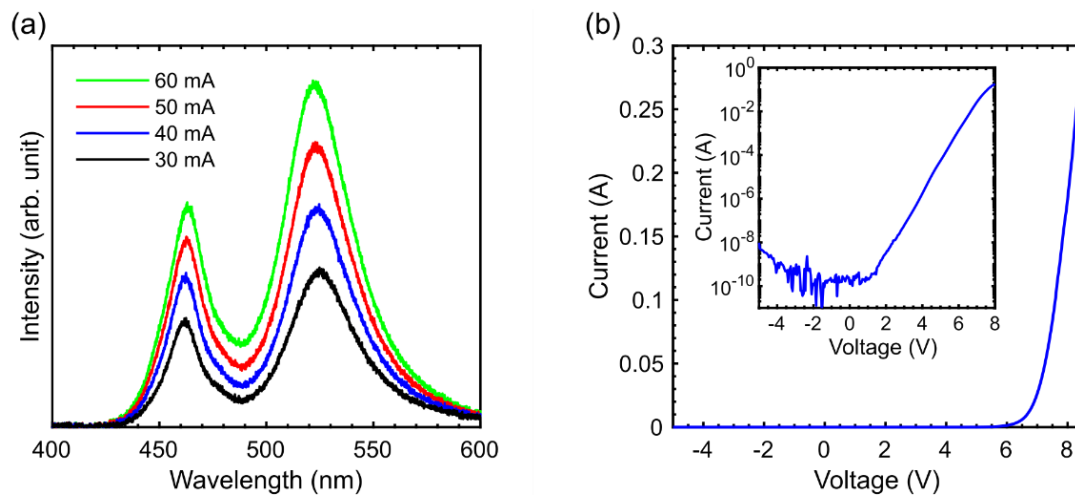

Figure 5. (**a**) The optical spectra of 2 LEDs connected by tunnel junction (TJ) for different driving currents. (**b**) The Current–Voltage (I–V) characteristics for the stack of 2 LEDs; inset to this figure is the same plot in semi-log scale and an indication of very low current leakage in reverse direction.
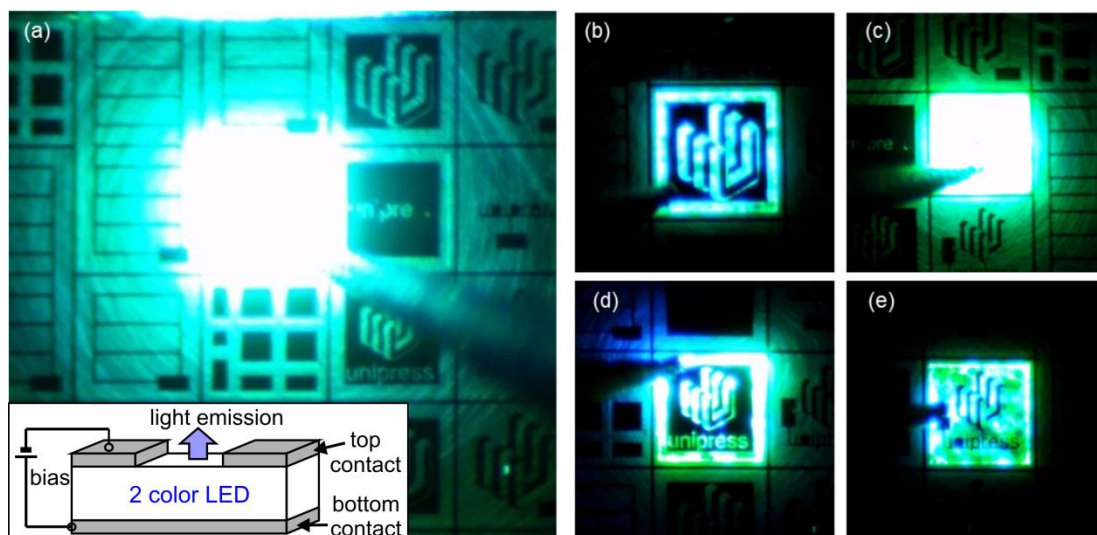

Figure 6. (**a**) The optical microscope image of operating multicolor TJ LEDs with full mesa size of 350×350 μm^2, surrounded by other devices. The devices have various geometry of upper metal contact; metallization blocks the light generated in the active region as schematically depicted in the insert and therefore the top contact pads are visible as black. When an LED chip is biased though a needle placed on top, the bright light emission is visible. (**b–e**) Operation of LEDs with different metallization patterns.
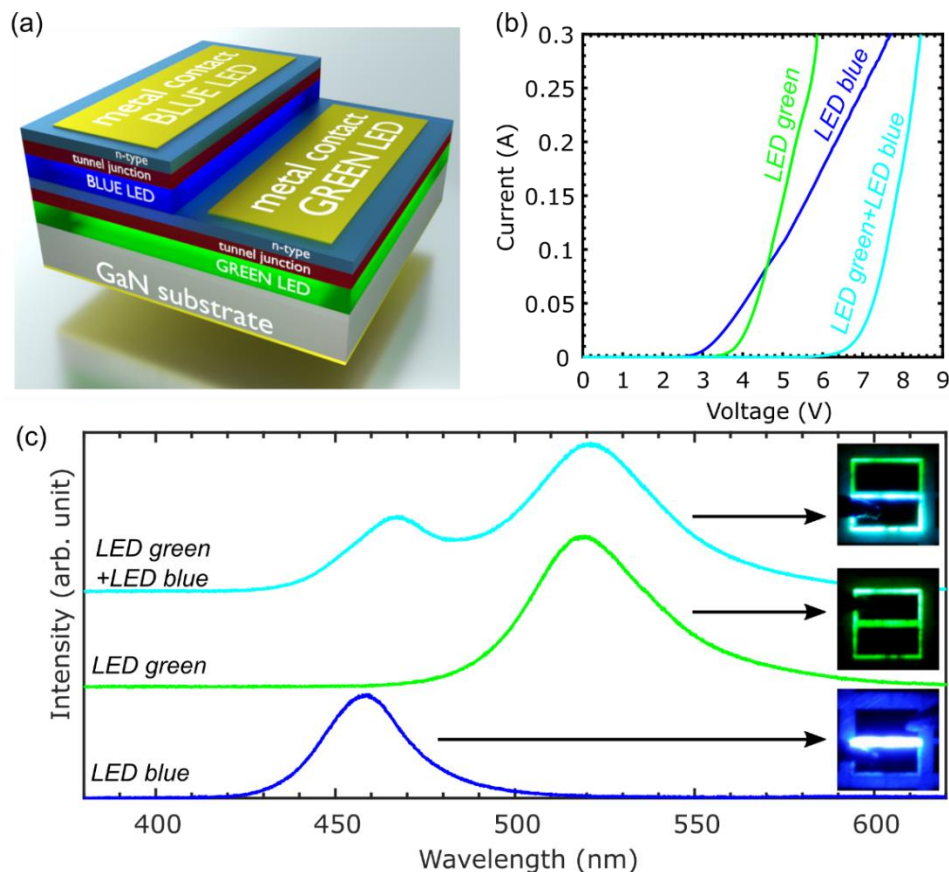
Figure 7. (**a**) Diagram of two LEDs after dry etching and contact deposition. (**b**) I–V and (**c**) spectral characteristics (together with true-color electroluminescence pictures) of blue, green and both LEDs.

4. Conclusions

We demonstrated a stack of four nitride LDs interconnected by TJs grown by PAMBE. We show that it is possible to grow four LDs with a structure almost 5 μm thick without lattice relaxation. Quality of epitaxy and design of TJ are reflected by low dislocation density at the level of low 10^6 cm^{-2}. The lasing wavelength is 453 nm. We show that three LDs are operating simultaneously, and the slope efficiency is increased three times. The first LD started to operate at 3.8 kA/cm^2 with SE equal to 0.8 W/A. When all three LDs were operating, the SE increased to 2.3 W/A. This result, together with the near-field pictures, is proof for simultaneous lasing of three LDs. Application of this design for *n*-LDs interconnected by (*n* − 1) TJ will allow us to increase SE *n*-times. The presented design is a viable alternative to achieving III-nitride high-power pulse laser diodes for many applications such as gas sensing or LIDARs.

We also investigate the stack of multicolor LEDs interconnected by TJs for white color, phosphorus-free LEDs and for LED array displays applications. The use of TJs simplifies the electrical connections to buried LED structures, eliminating the need of *p*-type contacts application.

Author Contributions: Conceptualization, M.S. (Marcin Siekacz), G.M. and C.S.; methodology, G.M.; investigation, M.S. (Marcin Siekacz), M.H., M.Ż., K.N.-S., S.S., M.C., J.S.-K. and A.F.-Ż.; resources, K.N.-S. and A.F.-Ż.; C.S. and M.S. (Marcin Siekacz); writing—original draft preparation, M.S. (Marcin Siekacz), C.S. and M.S. (Marta Sawicka); writing—review and editing, M.S. (Marcin Siekacz), G.M., H.T., M.H., M.C., M.S. (Marta Sawicka) and C.S.; visualization, M.S. (Marta Sawicka), M.H., M.Ż.; supervision, C.S. All authors have read and agreed to the published version of the manuscript.

Conflicts of Interest: The authors declare no conflict of interest.

References

1.   Nakamura, S.; Fasol, G.; Pearton, S. *The Blue Laser Diode: The Complete Story*; Springer: Berlin, Germay, 2000.

2.   Esaki, L. New phenomenon in narrow germanium $p-n$ junctions. *Phys. Rev.* **1958**, *109*, 603–604. [CrossRef]

3.   Krishnamoorthy, S.; Akyol, F.; Rajan, S. InGaN/GaN tunnel junctions for hole injection in GaN light emitting diodes. *Appl. Phys. Lett.* **2014**, *105*, 141104. [CrossRef]

4.   Leonard, J.T.; Young, E.C.; Yonkee, B.P.; Cohen, D.A.; Margalith, T.; DenBaars, S.P.; Speck, J.S.; Nakamura, S. Demonstration of a III-nitride vertical-cavity surface-emitting laser with a III-nitride tunnel junction intracavity contact. *Appl. Phys. Lett.* **2015**, *107*, 091105. [CrossRef]

5.   Malinverni, M.; Tardy, C.; Rossetti, M.; Castiglia, A.; Duelk, M.; Vélez, C.; Martin, D.; Grandjean, N. InGaN laser diode with metal-free laser ridge using n+-GaN contact layers. *Appl. Phys. Express* **2016**, *9*, 061004. [CrossRef]

6.   Kuwano, Y.; Kaga, M.; Morita, T.; Yamashita, K.; Yagi, K.; Iwaya, M.; Takeuchi, T.; Kamiyama, S.; Akasaki, I. Lateral Hydrogen Diffusion at p-GaN Layers in Nitride-Based Light Emitting Diodes with Tunnel Junctions. *Jpn. J. Appl. Phys.* **2013**, *52*, 08jk12. [CrossRef]

7.   Krishnamoorthy, S.; Nath, D.N.; Akyol, F.; Park, P.S.; Esposto, M.; Rajan, S. Polarization-engineered GaN/InGaN/GaN tunnel diodes. *Appl. Phys. Lett.* **2010**, *97*, 203502. [CrossRef]

8.   Malinverni, M.; Martin, D.; Grandjean, N. InGaN based micro light emitting diodes featuring a buried GaN tunnel junction. *Appl. Phys. Lett.* **2015**, *107*, 051107. [CrossRef]

9.   Diagne, M.; He, Y.; Zhou, H.; Makarona, E.; Nurmikko, A.V.; Han, J.; Waldrip, K.E.; Figiel, J.J.; Takeuchi, T.; Krames, M. Vertical cavity violet light emitting diode incorporating an aluminum gallium nitride distributed Bragg mirror and a tunnel junction. *Appl. Phys. Lett.* **2001**, *79*, 3720–3722. [CrossRef]

10.   Kurokawa, H.; Kaga, M.; Goda, T.; Iwaya, M.; Takeuchi, T.; Kamiyama, S.; Akasaki, I.; Amano, H. Multijunction GaInN-based solar cells using a tunnel junction. *Appl. Phys. Express* **2014**, *7*, 034104. [CrossRef]

11.   Czernecki, R.; Grzanka, E.; Jakiela, R.; Grzanka, S.; Skierbiszewski, C.; Turski, H.; Perlin, P.; Suski, T.; Donimirski, K.; Leszczynski, M. Hydrogen diffusion in GaN:Mg and GaN:Si. *J. Alloys Compd.* **2018**, *747*, 354–358. [CrossRef]

12.   Jeon, S.-R.; Song, Y.-H.; Jang, H.-J.; Yang, G.M.; Hwang, S.W.; Son, S.J. Lateral current spreading in GaN-based light-emitting diodes utilizing tunnel contact junctions. *Appl. Phys. Lett.* **2001**, *78*, 3265–3267. [CrossRef]

13.   Neugebauer, J.; Van de Walle, C.G. Role of hydrogen in doping of GaN. *Appl. Phys. Lett.* **1996**, *68*, 1829–1831. [CrossRef]

14.   Skierbiszewski, C.; Muziol, G.; Nowakowski-Szkudlarek, K.; Turski, H.; Siekacz, M.; Feduniewicz-Zmuda, A.; Nowakowska-Szkudlarek, A.; Sawicka, M.; Perlin, P. True-blue laser diodes with tunnel junctions grown monolithically by plasma-assisted molecular beam epitaxy. *Appl. Phys. Express* **2018**, *11*, 034103. [CrossRef]

15.   Schwarz, B. Mapping the world in 3D. *Nat. Photonics* **2010**, *4*, 429–430. [CrossRef]

16.   Okawara, S.; Aoki, Y.; Kuwabara, M.; Takagi, Y.; Maeda, J.; Yoshida, H. Nitride-based stacked laser diodes with a tunnel junction. *Appl. Phys. Express* **2018**, *11*, 012701. [CrossRef]

17.   Siekacz, M.; Muziol, G.; Hajdel, M.; Żak, M.; Nowakowski-Szkudlarek, K.; Turski, H.; Sawicka, M.; Wolny, P.; Feduniewicz-Żmuda, A.; Stanczyk, S.; et al. Stack of two III-nitride laser diodes interconnected by a tunnel junction. *Opt. Express* **2019**, *27*, 5784–5791. [CrossRef] [PubMed]

18.   Dwiliński, R.; Doradziński, R.; Garczyński, J.; Sierzputowski, L.P.; Puchalski, A.; Kanbara, Y.; Yagi, K.; Minakuchi, H.; Hayashi, H. Bulk ammonothermal GaN. *J. Cryst. Growth* **2009**, *311*, 3015–3018. [CrossRef]

19.   Muziol, G.; Turski, H.; Siekacz, M.; Szkudlarek, K.; Janicki, L.; Baranowski, M.; Zolud, S.; Kudrawiec, R.; Suski, T.; Skierbiszewski, C. Beyond Quantum Efficiency Limitations Originating from the Piezoelectric Polarization in Light-Emitting Devices. *ACS Photonics* **2019**, *6*, 1963–1971. [CrossRef]

20.   Skierbiszewski, C.; Turski, H.; Muziol, G.; Siekacz, M.; Sawicka, M.; Cywiński, G.; Wasilewski, Z.R.; Porowski, S. Nitride-based laser diodes grown by plasma-assisted molecular beam epitaxy. *J. Phys. D Appl. Phys.* **2014**, *47*, 073001. [CrossRef]

21. Siekacz, M.; Szańkowska, M.Ł.; Feduniewicz-Zmuda, A.; Smalc-Koziorowska, J.; Cywiński, G.; Grzanka, S.; Wasilewski, Z.R.; Grzegory, I.; Łucznik, B.; Porowski, S.; et al. InGaN light emitting diodes for 415 nm-520 nm spectral range by plasma assisted MBE. *Phys. Status Solidi C* **2009**, *6*, S917–S920. [CrossRef]

22. Sarzyński, M.; Kryśko, M.; Targowski, G.; Kamler, G.; Domagała, J.; Czernecki, R.; Libura, A.; Perlin, P.; Leszczyński, M. Nitride based laser diodes on substrates with patterned AlN mask. *Appl. Phys. Lett.* **2007**, *91*, 221103. [CrossRef]

23. Rogowsky, S.; Braun, H.; Schwarz, U.T.; Brüninghoff, S.; Lell, A.; Strauß, U. Multidimensional near- and far-field measurements of broad ridge (Al,In)GaN laser diodes. *Phys. Status Solidi C* **2009**, *6*, S852–S855. [CrossRef]

24. Scholz, D.; Braun, H.; Schwarz, U.T.; Brüninghoff, S.; Queren, D.; Lell, A.; Strauss, U. Measurement and simulation of filamentation in (Al,In)GaN laser diodes. *Opt. Express* **2008**, *16*, 6846–6859. [CrossRef] [PubMed]

25. Okumura, H.; Martin, D.; Malinverni, M.; Grandjean, N. Backward diodes using heavily Mg-doped GaN growth by ammonia molecular-beam epitaxy. *Appl. Phys. Lett.* **2016**, *108*, 072102. [CrossRef]

26. Kaufmann, U.; Schlotter, P.; Obloh, H.; Köhler, K.; Maier, M. Hole conductivity and compensation in epitaxial GaN: Mg layers. *Phys. Rev. B* **2000**, *62*, 10867–10872. [CrossRef]

27. Muziol, G.; Siekacz, M.; Nowakowski-Szkudlarek, K.; Hajdel, M.; Smalc-Koziorowska, J.; Feduniewicz-Żmuda, A.; Grzanka, E.; Wolny, P.; Turski, H.; Wiśniewski, P.; et al. Extremely long lifetime of III-nitride laser diodes grown by plasma assisted molecular beam epitaxy. *Mater. Sci. Semicond. Process.* **2019**, *91*, 387–391. [CrossRef]